ARTICLE IN PRESS

JGLR-01088; No. of pages: 13; 4C: 9, 11

Journal of Great Lakes Research xxx (2016) xxx–xxx

Contents lists available at ScienceDirect

Journal of Great Lakes Research

journal homepage: www.elsevier.com/locate/jglr

Simulating the effect of nutrient reduction on hypoxia in a large lake (Lake Erie, USA-Canada) with a three-dimensional lake model

Serghei A. Bocaniov [a,*], Luis F. Leon [b], Yerubandi R. Rao [b], David J. Schwab [a], Donald Scavia [a]

[a] Graham Sustainability Institute, University of Michigan, Ann Arbor, MI, USA
[b] S&T/WHERD/Integrated Modelling, Environment Canada, Burlington, Canada

ARTICLE INFO

Article history:
Received 30 December 2015
Accepted 26 May 2016
Available online xxxx

Communicated by Joseph DePinto

Index words:
Lake Erie
Hypoxia
Nutrient loads
Phosphorus
Ecological modeling
Hydrodynamic modeling

ABSTRACT

Hypoxia, or low dissolved oxygen (DO) concentrations, in lakes is commonly linked to eutrophication caused by excessive nutrient loadings. While nutrient-driven eutrophication creates a potential for hypoxia, the full realization of this potential, as well as its location, ultimate size, and duration, is to a large degree dependent on the lake's physics. Herein, we employed a three-dimensional coupled hydrodynamic and ecological model of Lake Erie to explore the potential for spatial and temporal developments of hypoxia and its response to nutrient load reductions. Reducing loads by 40 to 50% relative to the 2008 load will result in significant reductions (~50%) of hypoxia in terms of its maximum and mean areal extents and duration, as well as providing significant improvements in mean hypolimnetic DO. We also explored the impact of different DO threshold concentrations to characterize hypoxia, and found that responses at lower thresholds are most sensitive to variation in nutrient loads.

Introduction

Productive and thermally/chemically stratified lakes, estuaries and coastal systems are susceptible to developing hypoxic conditions (low dissolved oxygen concentrations) and sometimes reaching their more severe conditions, anoxia (absence or very low dissolved oxygen), with implications at both global and local levels. Under very low oxygen conditions, aquatic respiration becomes successively based on nitrate, manganese, iron (hydr)oxides and sulfate, thus altering key biogeochemical cycles (Pena et al., 2010). Moreover, anoxic conditions contribute to formation of methane (CH_4), a strong green-house gas, rather than carbon dioxide (CO_2), a weaker green-house gas produced when more oxygen is present (Bastviken et al., 2004). The areal flux of CH_4 can be a significant source in large and shallow systems like Lake Erie (Bastviken et al., 2004). Elevated concentrations of manganese mobilized from anoxic sediments also require additional drinking water treatment for its removal (Sly et al., 1990). However, one of the most significant local effects manifests through altering survival, behavioral, physiological, growth, and reproductive responses of aquatic biota including shellfish, benthic invertebrates and fishes (Carlson et al., 1980; Roberts et al., 2009; Vanderploeg et al., 2009; Arend et al., 2011; Roberts et al., 2011).

Lake Erie has a long history of eutrophication linked to excessive nutrient loads, with especially high loads occurring in the 1960s through 1980s (Electronic Supplementary material (ESM) Fig. S1). In response, the 1978 Great Lakes Water Quality Agreement (GLWQA) between United States and Canada established target loads for phosphorus (P) for each of the Great Lakes (IJC, 1978). The target load for Lake Erie total phosphorus (TP) was 11,000 MTA (metric tons per annum) that, at that time, was thought to be sufficient to improve areas of low dissolved oxygen (DO) and reduce or eliminate harmful algal blooms. As a result, annual TP loads were reduced from nearly 30,000 MTA in the late 1970s to about 11,000 MTA, with an average load over the past 20 years of about 9,000 MTA (ESM Fig. S1). However, despite the significant reduction in nutrient loads since the mid-1990s, Lake Erie began to experience a resurgence of large hypoxic zones (Hawley et al., 2006; Zhou et al., 2013, 2015; Scavia et al., 2014; Bocaniov and Scavia, 2016), including a recent record-breaking hypoxic extent in 2012 (Zhou et al., 2015). In response, the 2012 GLWQA agreement (IJC, 2012) called for a review and, if necessary, revision of the 1978 targets.

Previous efforts to simulate bottom water dissolved oxygen concentrations in Lake Erie included a wide range of models; from simplified box-reactor-type models (e.g. Di Toro et al., 1987; Lam et al., 1987, 2008) to more complex and spatially resolved 1-dimensional (1D) and 2D models (e.g. Rucinski et al., 2014; Boegman, 2006; Zhang et al., in this issue). While these efforts improved our understanding and

* Corresponding author.
E-mail addresses: bocaniov@umich.edu, serghei.bocaniov@gmail.com (S.A. Bocaniov).

http://dx.doi.org/10.1016/j.jglr.2016.06.001
0380-1330/

Please cite this article as: Bocaniov, S.A., et al., Simulating the effect of nutrient reduction on hypoxia in a large lake (Lake Erie, USA-Canada) with a three-dimensional lake model, J. Great Lakes Res. (2016), http://dx.doi.org/10.1016/j.jglr.2016.06.001

predictability of hypoxia, their simplified representations of physical processes, bathymetry and atmospheric forcing limited their ability to explore the complex lake thermodynamic and hydrodynamic processes and patterns, including the effects of density currents, Coriolis force, and enhanced mixing due to actions of internal waves and boundary mixing.

The earlier models were thus not designed to simulate spatial development and location of hypoxia. Yet, observations of Lake Erie's hypoxic conditions (e.g. Kraus et al., 2015) suggest a highly dynamic hypoxic zone that can be patchy and driven by dynamic physical processes such as general lake circulation (Beletsky et al., 2012), near-inertial internal waves (Bouffard et al., 2012), and extreme events such as upwelling-induced mixing (e.g. Rao et al., 2014; Bocaniov et al., 2014b). Resolving these processes requires a model capable of representing in-lake physical processes, basin topography and, heterogeneous atmospheric conditions. Thus, the major objective of this study was to employ a coupled hydrodynamic-ecological 3D model to develop a relationship between external phosphorus loads and the spatial and temporal dynamics of hypoxia in Lake Erie.

Methods and materials

Study site

Lake Erie is a very large, shallow lake (mean depth = 18.9 m) with a surface area of 25,657 km^2 and a volume of 484 km^3 (Bolsenga and Herdendorf, 1993) located in the temperate zone of North America between latitudes [41–43°N] and longitudes [79–83.5°W]. The lake has three distinct basins (Fig. 1). Its central basin is the largest with a volume of 305 km^3 and an area of 16,138 km^2 (Bolsenga and Herdendorf, 1993), stretching 213 km in length and 92 km in width, with a very flat bottom and mean and maximum depths of 18.5 and 25.6 m, respectively. The water retention capacity of the central basin is 1.74 years, compared with 2.76 years for the entire lake (Bolsenga and Herdendorf, 1993). The central basin experiences extensive, seasonally re-occurring hypoxia (Zhou et al., 2013, 2015), particularly during the period of late September through early October when it is interrupted by autumnal lake overturn as a result of the combined effects of the weakened water column stability due to lower surface water temperatures and increased intensity of mixing due to autumnal storms. For our purposes, we set the western boundary of the central basin as a straight line from Pelee Point to the edge of Sandusky Bay and the eastern boundary as a line along the natural ridge separating east and central basins, called Long Point Lake Erie Ridge (Fig. 1).

Hydrodynamic and ecological model

The model we used is the 3D coupled hydrodynamic and ecological model ELCOM-CAEDYM. The hydrodynamic Estuary and Lake COmputer Model (ELCOM; Hodges et al., 2000; Hodges and Dallimore, 2006) is designed for numerical simulation of hydrodynamics/thermodynamics of stratified inland and coastal waters. It accounts for baroclinic effects, earth's rotation (Coriolis force), meteorological forcing, inflows and outflows. It is dynamically coupled with the Computational Aquatic Ecosystem DYnamics Model (CAEDYM; Hipsey, 2008) to simulate water and sediment chemical and biological processes. ELCOM provides CAEDYM with temperature, solar radiation, mixing, advection, and diffusion, while CAEDYM provides ELCOM with variations in light attenuation due to concentrations of dissolved and particulate organic matter, phytoplankton, and suspended solids. ELCOM-CAEDYM (ELCD) has been applied to Lake Erie to investigate nutrient and phytoplankton dynamics (e.g. Leon et al., 2011), ice extent and thickness and their effects on spring phytoplankton and DO concentrations (Oveisy et al., 2014), the effects of atmospheric forcing on thermal structure (Liu et al., 2014), the impacts of mussel grazing on phytoplankton biomass (Bocaniov et al., 2014a), and hypoxic extent as a function of bottom water DO concentration (Bocaniov and Scavia, 2016).

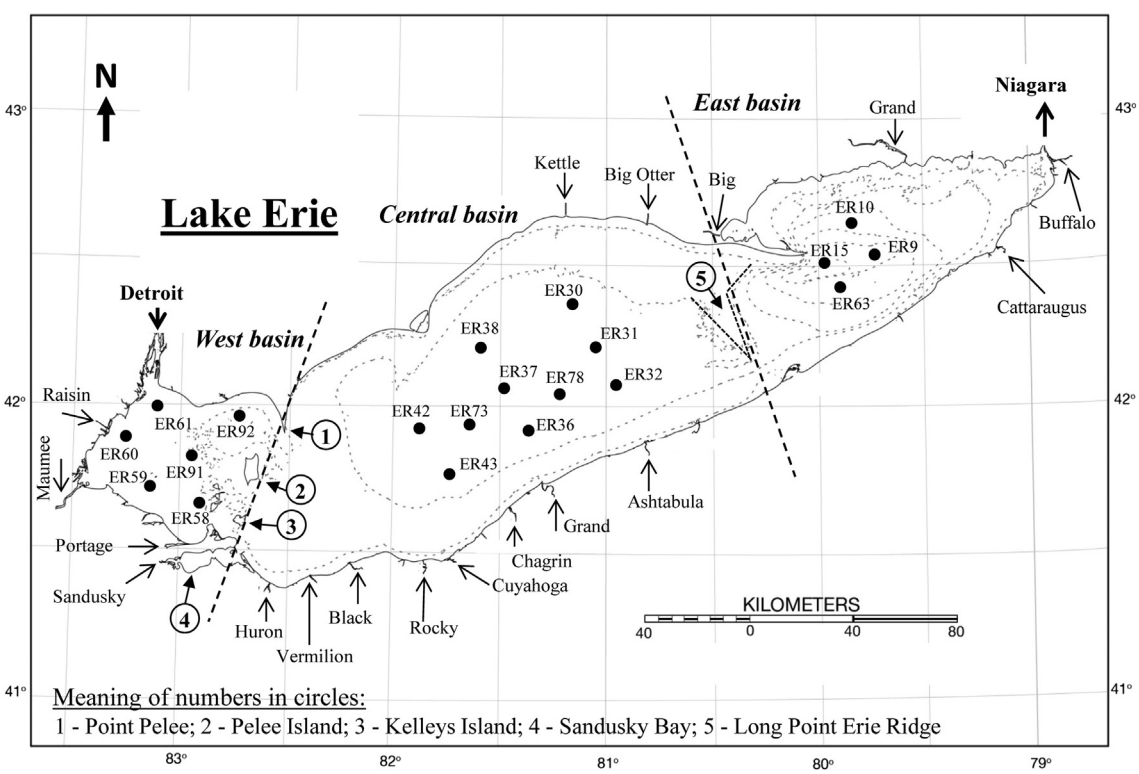

Fig. 1. Map of Lake Erie showing the central basin boundaries, included outflow and inflows (indicated by arrows), and the locations of the United States EPA stations (black solid circles). Dotted lines represent 10-m contours.

Please cite this article as: Bocaniov, S.A., et al., Simulating the effect of nutrient reduction on hypoxia in a large lake (Lake Erie, USA-Canada) with a three-dimensional lake model, J. Great Lakes Res. (2016), http://dx.doi.org/10.1016/j.jglr.2016.06.001

The ecological model CAEDYM includes representation of full cycles of the dissolved oxygen, carbon, phosphorus, nitrogen, silica, as well as simulation of two groups of suspended inorganic solids. CAEDYM has several biological components and can simulate up to seven phytoplankton groups, five zooplankton groups, six fish groups, four macroalgae groups, three invertebrate groups, three groups of mussels or clams, and one group of macrophytes, seagrass and jellyfish. There is flexibility upon the user decision for which species to include in a simulation. To reduce the complexity of the model and resulting possible uncertainties, in the current application we used three major nutrients (phosphorus, nitrogen and silica: P, N, Si) and five phytoplankton functional groups as in Leon et al. (2011). To correct for the grazing effects of zooplankton and mussels on phytoplankton biomass we increased the grazing-induced losses of the phytoplankton. More detailed information on CAEDYM including all state and rate equations and description of the modeled processes can be found elsewhere (e.g. Hipsey, 2008; ESM Tables S1, S2 & S3).

The computational grid was based on the detailed bathymetry of Lake Erie obtained from the NOAA National Geophysical Data Center. The 3D Cartesian mesh of the computational domain is comprised of 87 × 193 (16,791) 2 km square cells in the horizontal plane, each with 45 unevenly spaced vertical layers (0.5 to 5 m), but particularly in the central basin, with a maximum depth of 25.6 m, vertical layer thickness within this depth varied between 0.5 and 1 m. Of the 755,595 cells in the grid, only about 22% (165,999) are water cells used in the actual computations. The model was run for 190 days between April 21 and October 28, 2008 with a time step of 300 s. Initial conditions were set similar to its previous applications (e.g. Liu et al., 2014; Bocaniov and Scavia, 2016) with the initial spring in-lake conditions for physical, biological, and chemical properties based on water quality profiles measured at twenty USEPA stations (Fig. 1) during the April 2008 cruise.

The model accounts for nineteen major tributaries and one major outflow, the Niagara River (Fig. 1; Table 1), which also includes the Welland Canal discharge. Daily flows, water temperatures, and concentrations of water quality constituents were gathered from various sources, including Water Survey of Canada (Environment Canada), the Provincial Water Quality Monitoring Network (PWQMN; Ontario, Canada), Grand River Conservation Authorities (GRCA; Ontario, Canada), Heidelberg College Water Quality Laboratory, Michigan Department of Environmental Quality (MDEQ), United States Geological Survey (USGS), Great Lakes Environmental Research Laboratory's (GLERL), the STOrage and RETrieval system for water quality monitoring database (STORET) of USEPA, and other state agencies. Direct and indirect municipal and industrial discharges located downstream of the tributary water quality monitoring sites were gathered from the USEPA Permit Compliance System (PCS) and Ontario Ministry of Environment (Canada) with loads added to each corresponding tributary. Our independent calculation of external phosphorus loads for 2008 are similar to those calculated within the EcoFore project (http://www.ecofore.org) and those of Maccoux and Dove (in this issue).

Table 1
List of tributaries included in the model and their flows and total and dissolved reactive phosphorus (TP, DRP) loads in metric tons (MT) from April 21 (DOY 112) to October 28 (DOY 302) inclusive for the baseline scenario.

#	Tributary	Basin	TP load (MT)	DRP load (MT)	Average flow (±SD) ($m^3 s^{-1}$)	Range: min and max flow ($m^3 s^{-1}$)
1	Detroit	West	1240.33	689.30	5203.0 ± 188.0	4663.5–5617.8
2	Raisin	West	72.52	19.05	17.64 ± 26.29	2.44–172.45
3	Maumee	West	518.73	158.03	95.98 ± 118.84	3.40–515.37
4	Portage	West	60.29	44.49	7.07 ± 11.59	0.24–60.60
5	Sandusky	Central	175.20	37.71	21.88 ± 29.53	1.08–131.39
6	Huron [Ohio]	Central	28.41	8.61	6.88 ± 10.76	0.49–62.66
7	Vermilion	Central	28.09	9.16	5.52 ± 11.68	0.09–106.75
8	Black	Central	45.34	9.38	7.92 ± 17.97	0.28–138.75
9	Rocky	Central	38.63	16.89	1.58 ± 1.31	0.15–6.34
10	Cuyahoga	Central	173.26	55.75	17.13 ± 13.39	6.26–88.07
11	Chagrin	Central	53.43	30.49	6.48 ± 6.91	1.61–50.69
12	Grand [Ohio]	Central	32.35	7.62	11.04 ± 16.46	1.16–124.59
13	Ashtabula	Central	19.69	3.48	5[a]	n.a.
14	Cattaraugus	East	77.96	17.88	12.69 ± 11.6	3.65–84.10
15	Buffalo	East	38.66	9.75	8.34 ± 11.93	1.35–90.42
16	Grand [Ont.]	East	122.81	26.33	47.58 ± 28.19	24.20–231.00
17	Big	East	30.53	5.15	7.78 ± 2.44	3.93–15.68
18	Big Otter	East	17.45	4.20	4.68 ± 2.35	2.29–16.5
19	Kettle	East	5.34	1.98	0.72 ± 0.86	0.11–7.09
		Total	2779.02	1155.25		

[a] A constant daily flow was used for the Ashtabula River.

Meteorological forcing was applied to 13 approximately equal sized zones to account for variability across the lake (ESM Fig. S2). West and east basins were each divided into north and south zones, while the central basin was divided into nine approximately equal zones. Hourly observations of wind speed and direction, air temperature, relative humidity, solar radiation (shortwave), and cloud cover at 21 coastal stations and three in-lake buoys operated by the National Data Buoy Center and Environment Canada (ESM Fig. S2) were interpolated to the 13 zones following the approach described by Sambridge et al. (1995) with over-land/over-lake corrections developed for Lake Erie (e.g. Rodgers and Anderson, 1961; Schwab and Morton, 1984; Schertzer et al., 1987). Incoming longwave radiation was calculated for clear sky conditions and adjusted for cloud cover using the relationships of Idso and Jackson (1969) and Parkinson and Washington (1979). ESM Fig. S3 presents an example of meteorological data used for one of the thirteen meteorological forcing zones.

Model calibration and validation

The model was originally calibrated using the observed data for 2002 on thermal structure and several water quality constituents, such as nutrients, phytoplankton biomass, and seasonal succession of the major phytoplankton groups (Leon et al., 2011; Bocaniov et al., 2014a), and then validated for lake ice cover and thickness, water temperature, thermal structure and dissolved oxygen for 2005 (Oveisy et al., 2014) and 2008 (Liu et al., 2014). Herein, we extend that validation using higher resolution meteorological forcing and an increased number of tributaries (Fig. 1; Table 1). For water temperatures and DO concentrations, we used water quality profiles measured in the central basin by USEPA during seven cruises in 2008 (April 20–22, June 2–3; June 24–25; July 12–13; August 10–11; August 30–31; and, September 12–13). To validate surface water temperatures, we used satellite-derived lake-wide surface observations in 2008 available at the Great Lakes Surface Environmental Analysis (GLSEA) website (http://tinyurl.com/83tarmr, accessed May 12, 2015). For validation of water quality parameters such as phytoplankton biomass (Chl-*a*), total phosphorus (TP), reactive silica (RSi), nitrate (NO_3) and nitrite (NO_2) we used data from two basin-wide cruises from the Great Lakes Environmental database (GLENDA) available on the EPA Central Data Exchange (CDX) website [Web. 15 Nov. 2015. <https://cdx.epa.gov/epa_home.asp>].

In our analysis of hypoxia, we used several temporal and spatial characterizations: (i) maximum daily areal extent; (ii) average daily areal extent during the hypoxic summer (August 1 to September 30); (iii) average hypolimnetic DO concentration during the hypoxic summer; and, (iv) number of hypoxic days. Because the latter can be significantly inflated by small localized pockets of hypoxic areas, we used a threshold of 250 km^2 which represents <2% of the central basin area.

To calculate the average summer hypolimnetic DO, we defined the hypolimnion layer as any bottom cell during August and September with the following characteristics: (i) an average daily temperature ≤14.5 °C (maximum observed Lake Erie hypolimnion temperature); (ii) the difference between water surface and bottom temperatures >2 °C; and, (iii) DO concentration less than the defined hypoxia threshold. While a DO threshold of 2 mg L^{-1} is typically used to define

Please cite this article as: Bocaniov, S.A., et al., Simulating the effect of nutrient reduction on hypoxia in a large lake (Lake Erie, USA-Canada) with a three-dimensional lake model, J. Great Lakes Res. (2016), http://dx.doi.org/10.1016/j.jglr.2016.06.001

hypoxia, it has also been defined as values <5–6 mg L^{-1} (Farrell and Richards, 2009), with the majority of studies defining hypoxia between 0.3 and 4.0 (Vaquer-Sunyer and Duarte, 2008: $N = 49$ studies), and it has been shown that DO concentrations above 2 mg L^{-1} can affect behavior, reproduction, growth, and mortality of fishes and other organisms (Vaquer-Sunyer and Duarte, 2008; Vanderploeg et al., 2009; Arend et al., 2011). Therefore, we explored DO thresholds for hypoxic extent (HE) and duration, for thresholds of 1, 2, 3, and 4 mg L^{-1}.

Our main objective was to develop load-response curves for hypoxia characteristics with a base case with nutrient load close to the current Lake Erie target load of 11,000 MTA. In addition, because the water residence time of the central basin is about two years (>1.7 years), the water column nutrient concentrations in a given year are likely dependent on the preceding year's loads. Therefore, we selected for the base case a year where both that year and the previous year had nutrient loads close to 11,000 MTA. The years 1986 and 2008 both satisfy those conditions, but because 2008 is likely more representative of the current state, we used it as a base case scenario. This is the base year used by all of the other models in this multi-model effort (Scavia et al., in this issue).

Modeled scenarios

We conducted scenarios with seven different total phosphorus (TP) loadings: the 2008 base case ($TP_{100\%}$) and six scenarios representing different percent changes from the baseline: $TP_{125\%}$, $TP_{75\%}$, $TP_{60\%}$, $TP_{50\%}$, $TP_{25\%}$ and $TP_{0\%}$, where the subscripts represent the percent of the 2008 load. All scenarios used the same meteorology, water inflow and outflow water, and in-lake initial conditions. The only difference among scenarios was the adjusted tributary TP concentrations required to achieve the associated loading and the sediment oxygen demand (SOD) as described below.

Daily tributary TP loads were composed of dissolved reactive phosphorus (DRP, represented in the model as phosphate: PO_4), labile particulate organic phosphorous (POP), labile dissolved organic phosphorous (DOP), non-labile particulate inorganic phosphorous (PIP), and phosphorus content of the phytoplankton (IP). Each load scenario included the equal apportioning of daily concentrations of each fraction of TP for each individual tributary relative to its base case daily concentrations (Table 2).

Modeling sediment oxygen demand (SOD)

The full effect of nutrient load changes cannot be seen in the 190-day simulations used in our study because of the long-term deposition and accumulation of the organic matter (OM) in the lake sediments and, therefore, mismatch between the current OM deposition rate and sediment response to changes in that rate. Because the OM residence time in sediments is much longer than that in the water column, substantial time is needed before a new equilibrium is reached (Søndergaard et al., 2001, 2003). To approximate the effect of altered nutrient loads on SOD rates, they were adjusted as a function of those loads as has been done elsewhere for Lake Erie (Di Toro and Connolly, 1980; Rucinski et al., 2014, in this issue).

We specified the *SOD* rates (SOD_T; g O_2 m^{-2} day^{-1}) to be in equilibrium with the nutrient loads and to be spatially and temporally a function of temperature and *DO* concentration at sediment-water interface (Hipsey, 2008):

$$SOD_T = ASOD_{20} \cdot f(T) \cdot f(DO) = ASOD_{20} \cdot \theta^{T-20} \cdot \left[\frac{DO}{DO + K_{SOD}}\right] \quad (1)$$

where, SOD_T is the actual *SOD* rate used in the model (g O_2 m^{-2} day^{-1}), *T* is the water temperature (°C), *DO* is the dissolved oxygen concentration in the layer above sediments (mg L^{-1}), $ASOD_{20}$ is the maximum *SOD* rate at 20 °C (g O_2 m^{-2} day^{-1}) in equilibrium with the annual nutrient (phosphorus) load; θ is the temperature coefficient; and K_{SOD} is the constant that determines how the *SOD* is mediated under hypoxic conditions.

Our preliminary analysis indicated that a maximum *SOD* rate at 20 °C ($ASOD_{20}$) of 1.2 g O_2 m^{-2} d^{-1} results in similar SOD_T rates to those used by Rucinski et al. (2014) (ESM Table S4) and matches the seasonal dynamics of the observed *DO* concentrations in both the epilimnion and the hypolimnion. To determine $ASOD_{20}$ for each of the additional nutrient loading scenarios, we used the relationship between annual TP loads and sediment oxygen demand rates (see Fig. 10 in Rucinski et al., 2014). The calculated $ASOD_{20}$ values for each of the loading scenarios are shown in Table 2.

Table 2
Load scenario descriptions: tributary TP loads and maximum SOD rates at 20 °C ($ASOD_{20}$).

#	Phosphorus load scenario	Tributary TP load [relative to 2008 load] (%)	Max SOD rate[b] [$ASOD_{20}$] (gO_2 m^{-2} d^{-1})
1	$TP_{100\%}$[a]	100	1.200
2	$TP_{125\%}$	125	1.264
3	$TP_{75\%}$	75	1.106
4	$TP_{60\%}$	60	1.026
5	$TP_{50\%}$	50	0.957
6	$TP_{25\%}$	25	0.681
7	$TP_{0\%}$	0	0.559

[a] Base case.
[b] Maximum SOD rate at 20 °C ($ASOD_{20}$) is a value used by ELCD to calculate the actual SOD fluxes (SOD_T) depending on temperatures and DO concentrations of the layer just above sediments (see Eq. (1) for more details). See ESM Table S4 for comparison of the actual SOD_T values with the literature values for the base case scenario.

Results

Characterization of the thermal structure

Based on observations at locations of ten index USEPA stations in the central basin (Fig. 1), all three thermal structure layers were already present by the end of June with a formation of metalimnion with distinct boundaries. Over the observed season (end of June to early September; Table 3), the depths of the epilimnion, metalimnion and hypolimnion were increasing with mean monthly rates of about 1.2, 1.1 and 1.0 m per month, respectively. On average, the epilimnion was very thick (14.7 m; Table 3) compared to thinner metalimnion and hypolimnion layers (2.3 and 4.9 m, respectively). The volume of the epilimnion was very large occupying more than three quarters of the entire basin volume (78%) followed by the hypolimnetic and metalimnetic volumes (18% and 4%, respectively).

Validation and dynamics

Simulations of surface water temperatures (Fig. 2a), average epilimnetic temperatures (Fig. 2b), bottom temperatures (Fig. 2c), and bottom DO concentrations at the locations of the USEPA index stations (Fig. 2d), as well as basin-wide averages (Fig. 2e) were in a good agreement with observations. The ELCD model was able to represent the thermal structure correctly (Table 4). Though the simulated metalimnion was more diffusive than the measured one, the depth of the thermocline (the largest change in water densities) was very well captured (Table 4). Detailed comparisons for Chl-*a*, TP, RSi and $NO_2 + NO_3$ between simulated and observed results provided validation of the accuracy of the model predictions (Table 5; Fig. 3). The modeled estimates of hypoxic location, magnitude, onset, peak, and dissipation are also consistent with previous studies (Zhou et al., 2013, 2015).

Table 3
Characterization of the central Lake Erie thermal structure in summer 2008 (June 24–25 to September 12) with the corresponding depths, volumes, thicknesses and temperatures for each thermal stratum (epilimnion: *EPI*; metalimnion: *META*; thermocline: *THERMO*; hypolimnion: *HYPO*) and derived from the thermal structure observations during five basin-wide EPA summer cruises (see "Day/Month" column for dates). Numbers indicate mean ± SD with numbers in round brackets indicating percentage of the total lake volume. Number of observations (temperature profiles) for each cruise is ten. The thickness of the hypolimnion (*HYPO*) was determined by the division of the hypolimnetic volume by its surface area.

Day/Month	DOY	Depth (m)			Thickness (m)	
		EPI	*THERMO*	*HYPO*	*EPI*	*META*
24–25/06	176–177	13.2 ± 0.9	14.6 ± 1.0	15.6 ± 1.0	13. 2 ± 0.9	2.4 ± 0.6
12/07	194	13.4 ± 3.2	15.3 ± 2.6	16.5 ± 2.6	13.4 ± 3.2	3.1 ± 1.1
09–10/08	222–223	14.6 ± 2.5	15.5 ± 2.3	16.8 ± 2.2	14.6 ± 2.5	2.2 ± 0.8
30–31/08	243–244	16.1 ± 1.7	17.0 ± 1.7	18.0 ± 1.6	16.1 ± 1.7	1.9 ± 0.4
12/09	256	16.4 ± 1.8	17.4 ± 1.8	18.3 ± 1.6	16.4 ± 1.8	1.8 ± 0.6
Average		14.7 ± 1.5	15.9 ± 1.2	17.0 ± 1.1	14.7 ± 1.5	2.3 ± 0.5

Table 3. (*Continued*)

DOY	Volume (km^3)			Thickness (m)	Temperature (°C)	
	EPI	*META*	*HYPO*	*HYPO*	*EPI*	*HYPO*
176–177	212.1 (71.7%)	13.5 (4.5%)	70.4 (23.7%)	5.8	18.6 ± 0.3	9.8 ± 0.6
194	221.8 (74.9%)	14.2 (4.8%)	60.0 (20.2%)	5.4	21.7 ± 0.5	9.9 ± 0.9
222–223	224.4 (75.8%)	15.7 (5.2%)	55.9 (18.9%)	5.1	23.2 ± 0.5	11.1 ± 0.6
243–244	242.3 (81.9%)	10.9 (3.6%)	42.8 (14.4%)	4.3	22.1 ± 0.2	11.5 ± 1.0
256	246.8 (83.4%)	9.5 (3.2%)	39.7 (13.3%)	4.1	21.3 ± 0.2	11.5 ± 0.6
Average	*229.5 ± 14.6 (78%)*	*12.8 ± 2.5 (4%)*	*53.8 ± 12.6 (18%)*	*4.9 ± 0.7*	*21.4 ± 1.7*	*10.8 ± 0.8*

Our results show that the spatial and temporal extents of hypoxia are quite dynamic. Hypoxia first appeared in July (e.g. see Fig. 4a for HE_2: a hypoxic extent for DO threshold of 2 mg L^{-1}) as small isolated areas in the north-eastern part of the western basin and the north-western part of the central basin. Later in August, it completely disappears from the (fully mixed) west basin but continues growing in the

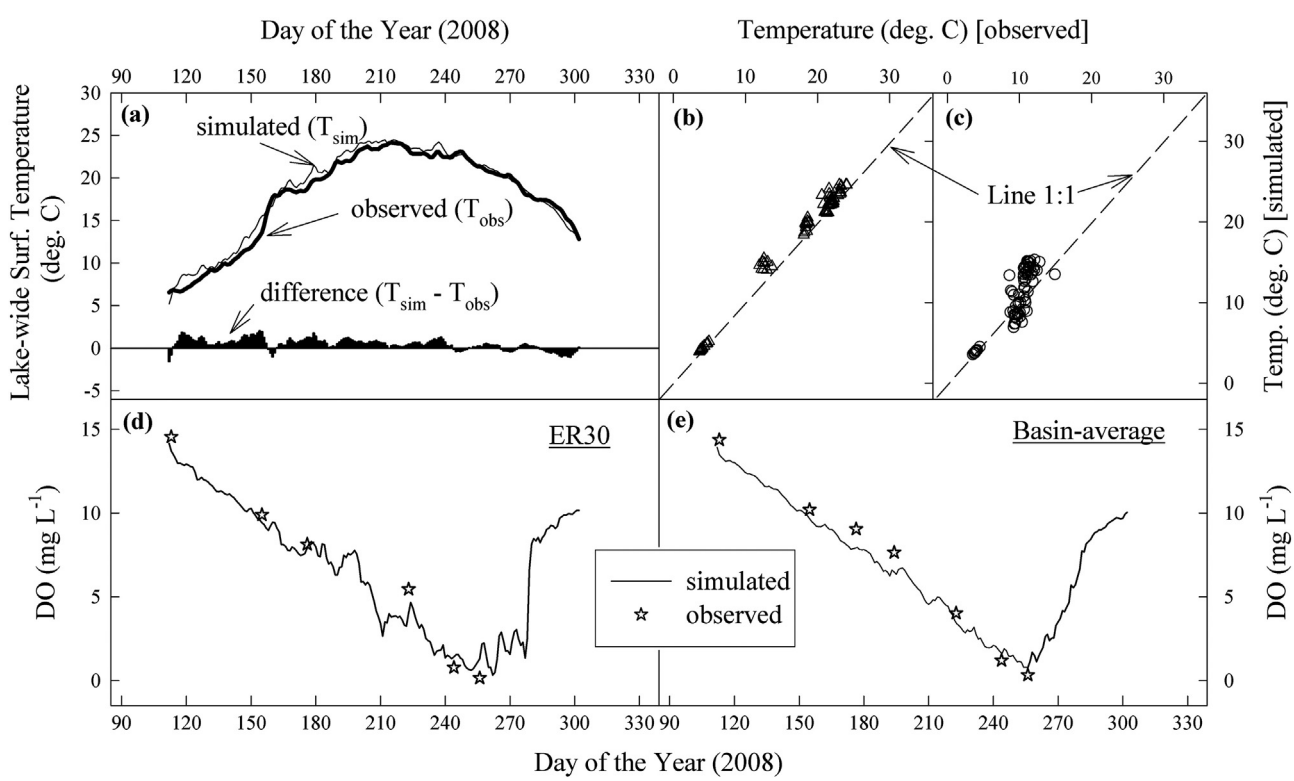

Fig. 2. Time-series of the observed and simulated daily lake-wide surface temperatures and their difference (a); plots of the observed vs simulated values of the temperatures averaged over the top 6 m of the surface mixed layer (b) and bottom temperatures (c); comparison of the simulated (solid line) and observed (open stars) bottom water DO at station ER30 (d); comparison of basin averaged simulated (solid line) and observed (open stars) bottom water DO (e).

Please cite this article as: Bocaniov, S.A., et al., Simulating the effect of nutrient reduction on hypoxia in a large lake (Lake Erie, USA-Canada) with a three-dimensional lake model, J. Great Lakes Res. (2016), http://dx.doi.org/10.1016/j.jglr.2016.06.001

Table 4
Characterization of the metalimnion layer vertical structure (mean depth ± SD) in central Lake Erie in 2008 based on the observations and numerical simulations for the locations of ten USEPA index stations (Fig. 1). The simulated values were compared to observations (measured temperature profiles) collected during five cruises in 2008 (June 24–25; July 12–13; August 10–11; August 30–31; and, September 12–13). Number of compared profiles is *N*.

#	Vertical structure of the metalimnion	Simulated depth: (m) $N = 50$	Observed depth: (m) $N = 50$
1.	Upper boundary	12.8 ± 2.8	14.7 ± 2.5
2.	Thermocline (maximum change in water density)	15.9 ± 3.1	15.9 ± 2.2
3.	Lower boundary	18.2 ± 2.5	17.0 ± 2.1

(stratified) central basin (Fig. 4b–e). As the season progresses, hypoxia extends to most of the central basin and reaches its maximum extent in early September (Figs. 4f–h & 5b), to finally dissipate in late September (Fig. 4i–l). Compared to HE_2, the spatial extent was smaller for HE_1 and larger for HE_3 and HE_4 (Fig. 5). The timing and duration periods were also different. HE_1 had the shortest duration and lasted for about six weeks from approximately mid-August to the end of September (Fig. 5a), while the durations for HE_3 and HE_4 were about three months (HE_3: mid-July to early October; HE_4: early July to early October). Temporal dynamics (formation and dissipation) were similar for all loading scenarios, lasting about two months with the exception of $TP_{25\%}$ and $TP_{0\%}$ (Fig. 5b).

Results also show that the areal extent and duration of hypoxia for all of the DO thresholds were sensitive and responsive to changes in nutrient loads (Figs. 6 & 7; ESM Figs. S4 & S5) with decreasing sensitivity for increasing DO thresholds (Fig. 5). HE_1 was the most sensitive (Fig. 5a), increasing in size for $TP_{125\%}$ and decreasing with the reductions in nutrient loads ($TP_{75\%}$, $TP_{50\%}$) and being trivial or absent for the $TP_{25\%}$ and $TP_{0\%}$ scenarios (Figs. 5a & 7). Hypoxic extent and duration for higher DO thresholds, HE_3 and HE_4, also responded to variations in nutrient loads (Fig. 5c–d) but were not as dynamic, especially for nutrient loads that did not deviate considerably from the base case (ESM Figs. S4 & S5).

The strong atmospheric forcing events (e.g. end of August 2008) had noticeable effects on hypoxia with the largest impacts on HE_1 and HE_2. These short, intense mixing events led to deeper mixing and increases in bottom DO and therefore decreased areal extent of hypoxia (e.g. late August and early September; Fig. 5). However, when stratification was restored, hypoxic extent increased. Overall, the hypoxic area moved in response to atmospheric forcing with a general circulation pattern reminiscent of that previously observed by Saylor and Miller (1987) in central Lake Erie (ESM Fig. S6).

Load-response curves

Load-response curves were developed for maximum and average hypoxic extent (Fig. 8a–b), mean summer (August–September) bottom layer hypolimnetic DO concentrations (Fig. 8c), and number of days with hypoxic area exceeding 1000 km^2 (Fig. 8d). The relationship between hypoxic extent and nutrient load is non-linear with large decreases in areal extent when nutrient loads are reduced by 40–50%. Hypoxic duration also responded to the phosphorus load reduction and was sensitive to the choice of the DO threshold used (Figs. 9 & 10; ESM Table S5).

Discussion

Although there have been previous studies of hypoxia in central Lake Erie, our work presents the first demonstration, through numerical modeling, of the three-dimensional basin-wide spatial and temporal dynamics of the seasonal hypoxia in Lake Erie, including its progression and overall seasonal duration. Our results showed that hypoxia sometimes has a patchy distribution, but can also be consolidated into a single large area. Unlike conventional understanding, our results suggest that hypoxia starts in the nearshore where the metalimnion is closer to the lake bottom and the hypolimnion is shallower and then moves offshore to the deeper mid-basin area, consolidating into one large area covering a large portion of the central basin with highly dynamic edges, consistent with recent field observations of high variability of hypoxic zone (Kraus et al., 2015). The scenario in which hypoxia starts in the nearshore may prevail under the dominant and more frequently observed circulation pattern in central Lake Erie which is cyclonic (counter-clockwise; Saylor and Miller, 1987; Beletsky et al., 2012) with the dome-shaped thermocline that is shallower offshore than in the nearshore leading to the conditions of the thick hypolimnion in the offshore. However, in years with anticyclonic (clockwise) circulation driven by anticyclonic vorticity in the surface wind (e.g. 2005; Beletsky et al., 2013) and formation of the bowl-shaped thermocline resulting in the thinner hypolimnion in the nearshore, hypoxia may start concurrently in some nearshore and offshore zones.

The lake circulation pattern and wind-induced extreme events such as downwelling and upwelling episodes have large effects on the spatial location of hypoxia. Unlike other systems with the spatially stable and cold (around 5 °C) hypolimnion with much larger volume of the hypolimntic water compared to the volume of epilimnion and with steep bottom topography (e.g. Rappbode Reservoir in central Germany; Bocaniov et al., 2014b), the volume of the hypolimnion in the central basin is very small compared to the overlaying volume of water (sum of epilimnion and metalimnion; Table 3), the hypolimnion is also warmer (e.g, mean T = 10.8 °C; Table 3) and therefore less dense than in other similar systems, and the bottom topography is very flat resulting in a very high sensitivity of the hypolimnion to any motion in the epilimnion. This highly sensitive nature and dynamic feature of Lake's Erie central basin hypolimnion and its coupling to the epilimnion via its dynamic response in terms of the spatial location and thickness to the prevailing wind-driven circulation in the epilimnion is very interesting to explore but deserves a more detailed separate study and will be addressed in the following study (Bocaniov and Scavia, in prep.).

Understanding both the location and seasonal progression of hypoxia is important both for interpreting monitoring results and advising management action. For example, knowing the spatial pattern of

Table 5
Summary of model performance statistics to evaluate the model ability to simulate water quality variables (Chl-*a*, chlorophyll-*a*; TP, total phosphorus; RSi, soluble reactive silica; $NO_3 + NO_2$, sum of nitrate and nitrite) observed at discrete sampling depths during EPA spring and summer cruises in 2008. *N*, number of compared pairs; *MEAN*, mean of the observations; SD_o, standard deviation of observations; *RE*, relative error; *RMSE*, root mean squared error; *RSR*, *RMSE*-observation standard deviation ratio (= $RMSE/SD_o$).

Parameter (units of measurement)	Lake-wide (entire lake) ($N = 206$)					Central basin ($N = 100$)				
	MEAN	SD_o	*RE*	*RMSE*	*RSR*	*MEAN*	SD_o	*RE*	*RMSE*	*RSR*
Chl-*a* (μg L^{-1})	4.78	4.04	0.27	1.67	0.41	6.53	4.79	0.26	1.85	0.39
TP (μg L^{-1})	11.39	10.63	0.21	3.02	0.28	10.22	4.58	0.17	2.01	0.44
RSi, (μg L^{-1})	415.58	381.67	0.32	223.19	0.58	305.27	401.84	0.49	268.91	0.67
$NO_3 + NO_2$ (μg L^{-1})	280.04	235.32	0.17	65.66	0.28	185.92	68.34	0.27	66.53	0.97

Please cite this article as: Bocaniov, S.A., et al., Simulating the effect of nutrient reduction on hypoxia in a large lake (Lake Erie, USA-Canada) with a three-dimensional lake model, J. Great Lakes Res. (2016), http://dx.doi.org/10.1016/j.jglr.2016.06.001

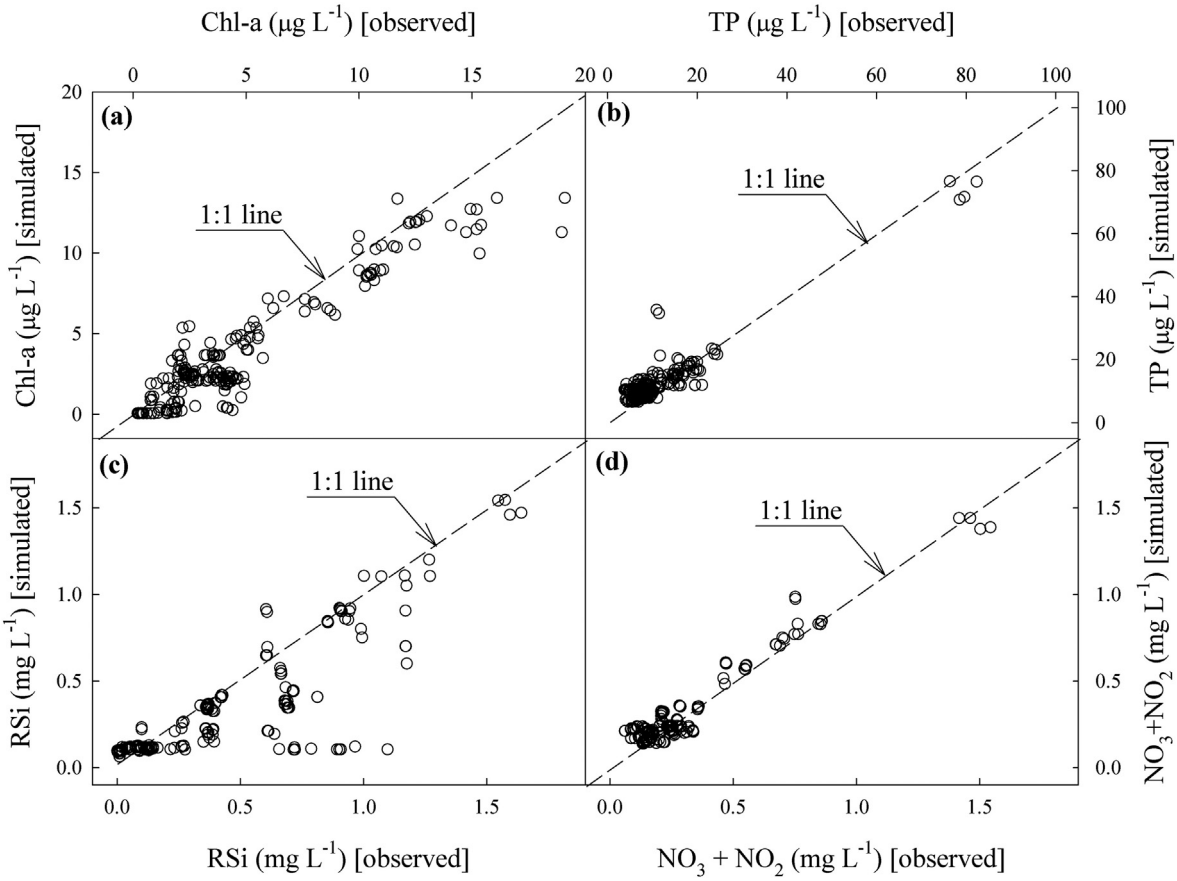

Fig. 3. Scatter plot of the lake-wide observed vs. simulated concentrations of chlorophyll-*a* (Chl-a; a), total phosphorus (TP; b), soluble reactive silica (RSi; c), and sum of nitrate and nitrite ($NO_3 + NO_2$; d) at all discrete sampling depths at the locations of twenty EPA index stations (see Fig. 1) sampled during spring and summer EPA cruises in 2008. Number of the compared pairs (N) for each water quality parameter is 206 ($N = 206$). See Table 5 for model performance statistics which is done separately for the entire lake and central basin.

hypoxia's seasonal progression may help design a more effective and less resource intensive field sampling program. Also, because hypoxia can overlap with areas of otherwise high quality benthic habitat that are most important to fish and used for spawning, larval development, nursery or foraging, the knowledge of the affected areas and the timing of the impact can help decisions to become more spatially directed and targeted as those, for example, currently being developed for the Chesapeake Bay management (CBMS, 2015).

Perhaps the most interesting result of this study is that the DO thresholds possess different degrees of sensitivity to variations in nutrient loads with an increasing sensitivity for lower thresholds. The latter are more sensitive to the external nutrient loads because they are smaller and therefore they are more responsive to any small addition or subtraction of the amount of DO to/from the system. For example, a decrease in 0.2 mg L^{-1} of the DO concentration will result in larger changes for a 1 mg L^{-1} threshold (−20%) than for a threshold of 4 mg L^{-1} (−5%). Therefore, the phosphorous loading reduction will be more effective at reducing areas with smaller, but more harmful and damaging, DO concentrations in respect to both reduced spatial extent and shortened duration (e.g. Figs. 8–10).

Another interesting result of our study is a high sensitivity of hypoxia to SOD rates. Volumetric hypolimnetic oxygen depletion (*VHOD*) that triggers and sustains hypoxic conditions is driven by the water column oxygen demand (*WOD*) and *SOD* and can be written as follows:

$$VHOD = WOD + \frac{SOD}{H} \tag{2}$$

where H is the thickness of the hypolimnion (m). It is seen from Eq. (2) that *VHOD* rates depend on the hypolimnetic thickness (H) and becomes larger for smaller H due to increasing contribution of *SOD* to *VHOD*. Previous studies on hypoxia in central Lake Erie (e.g. Bouffard et al., 2013) suggested that the contribution of *SOD* to *VHOD* equals that of *WOD* at the hypolimnetic thickness of about 6.6 m (e.g. ratio of mean *SOD* flux to mean *WOD*) and then starts to dominate over *WOD* as the hypolimnion becomes shallower. The central basin of Lake Erie has a very shallow hypolimnion with a mean thickness (= volume to area ratio) of much <6.6 m as judged from the field observations in 2008 (mean thickness = 4.9 m; June 24 to September 12, 2008; Table 3), therefore it is not surprising that under conditions of a very thin hypolimnetic layer, the development and maintenance of hypoxic conditions are more sensitive to *SOD* rather than *WOD*. As *SOD* represents long-term processes (historical deposition and accumulation of the OM in the sediments) and gives rates that are integrated over longer period of nutrient loads (from several years to perhaps decades) compared to *WOD* rates that are driven by the short-term process (photosynthesis) and therefore of very short duration (up to about five years), the high sensitivity of hypoxia to *SOD* in central basin of Lake Erie means that the hypoxia response to reduced external phosphorus loading is a slow process which can be further slowed and masked by the effects of climate warming and thermal lake response.

Central Lake Erie in its response to nutrient abatement is similar to many other shallow lakes with high historical nutrient loads. Many of these shallow lakes show delays in response to nutrient loads on the order of years to decades while water column and sediment phosphorus concentrations (or accumulated OM in the sediments) equilibrate to the new loads (Marsden, 1989; Jeppesen et al., 2005, 2007). Our results suggest that current *SOD* rates in central basin of Lake Erie are still relatively high and may still be responding to periods when nutrient loads where higher. As such, it might take considerable time until a new equilibrium

Please cite this article as: Bocaniov, S.A., et al., Simulating the effect of nutrient reduction on hypoxia in a large lake (Lake Erie, USA-Canada) with a three-dimensional lake model, J. Great Lakes Res. (2016), http://dx.doi.org/10.1016/j.jglr.2016.06.001

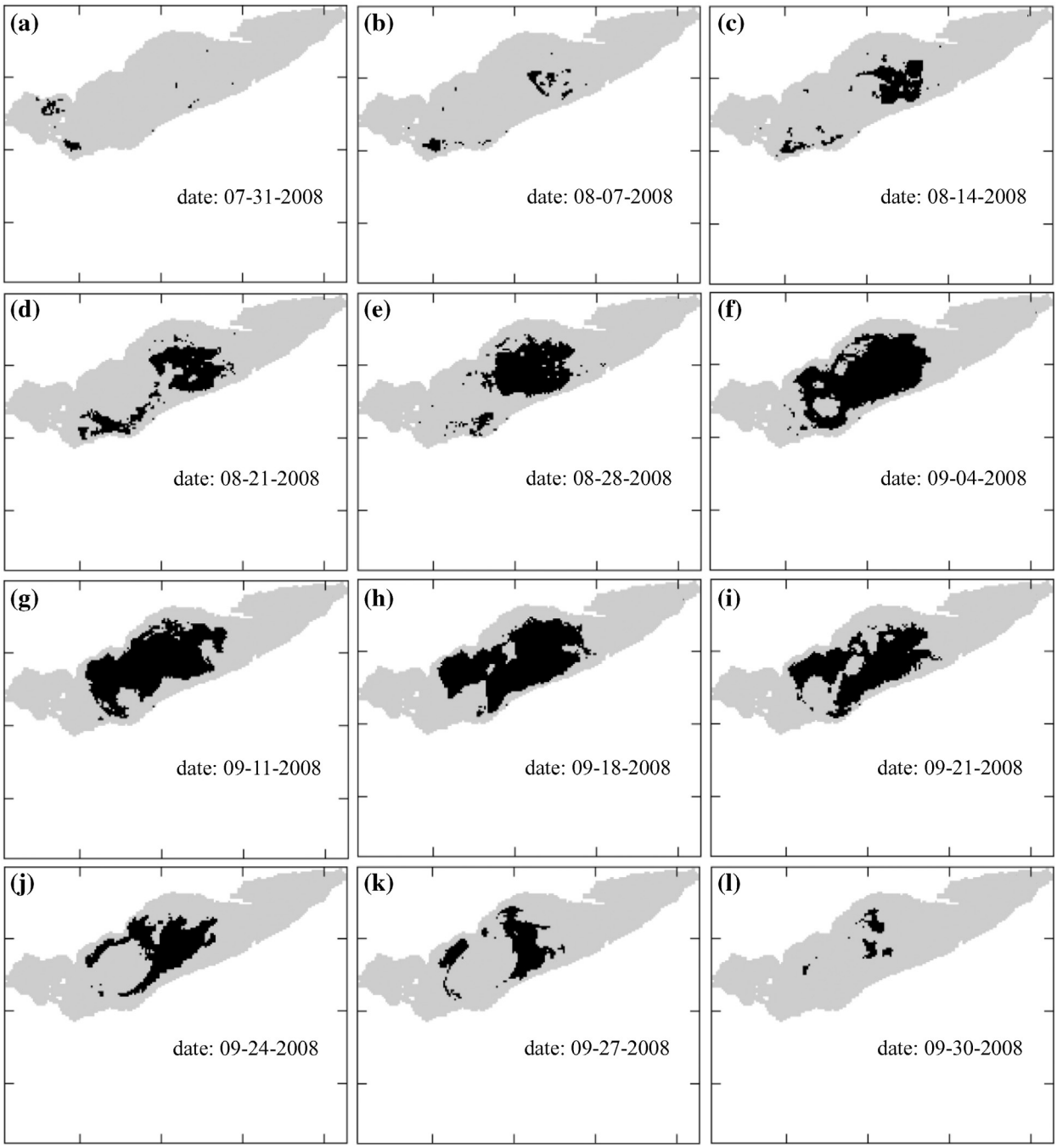

Fig. 4. Seasonal evolution of the spatial extent of hypoxia (HE_2, DO < 2 mg L^{-1}; indicated by black color) including its two major phases, development (a–g) and dissipation (h–l).

is reached between external nutrient loads and sediment fluxes so that the full effects of nutrient reduction can be seen.

We developed load-response curves, not only for the traditional 2 mg L^{-1} hypoxia threshold, but also for threshold concentrations of 1, 3, and 4 mg L^{-1} recognizing the importance of multi-threshold approaches in management of natural resources (Guntenspergen, 2014). Many aquatic organisms experience mortality at DO concentrations >2 mg L^{-1} (USEPA, 1986; Gray et al., 2002) so focusing on that threshold alone may underestimate a wide range of impacts. For example, studies show that 2 mg L^{-1} is below the sublethal and lethal oxygen threshold for about half of the aquatic organisms tested (Vaquer-Sunyer and Duarte, 2008) That is why other thresholds have been proposed (e.g., 3.5 mg L^{-1}, Steckbauer et al., 2011; 4.8 mg L^{-1}, Vaquer-Sunyer and Duarte, 2008), and are being tracked in Long Island Sound (State of Connecticut, 2015).

Our results show that hypoxic extent and duration, as well as mean summer hypolimnetic DO concentrations, are sensitive to nutrient load reduction, with the most significant changes associated with reductions of 40 to 50% from the 2008 levels (Fig. 8a-b). In addition, those responses are sensitive to what DO threshold is used. For example, a 40% load reduction results in simulated maximum hypoxic extents being reduced by 37.3% (2400 km^2), 19.1% (1700 km^2), 13.5% (1400 km^2) and 11.0% (1300 km^2) for HE_1, HE_2, HE_3 and HE_4, respectively (Fig. 8a). While a 50% reduction in nutrient load will result in 1.5 times larger percent reductions by 58.4%, 27.2%, 21.2% and 15.2% for HE_1, HE_2, HE_3 and HE_4, respectively. Compared to the maximum

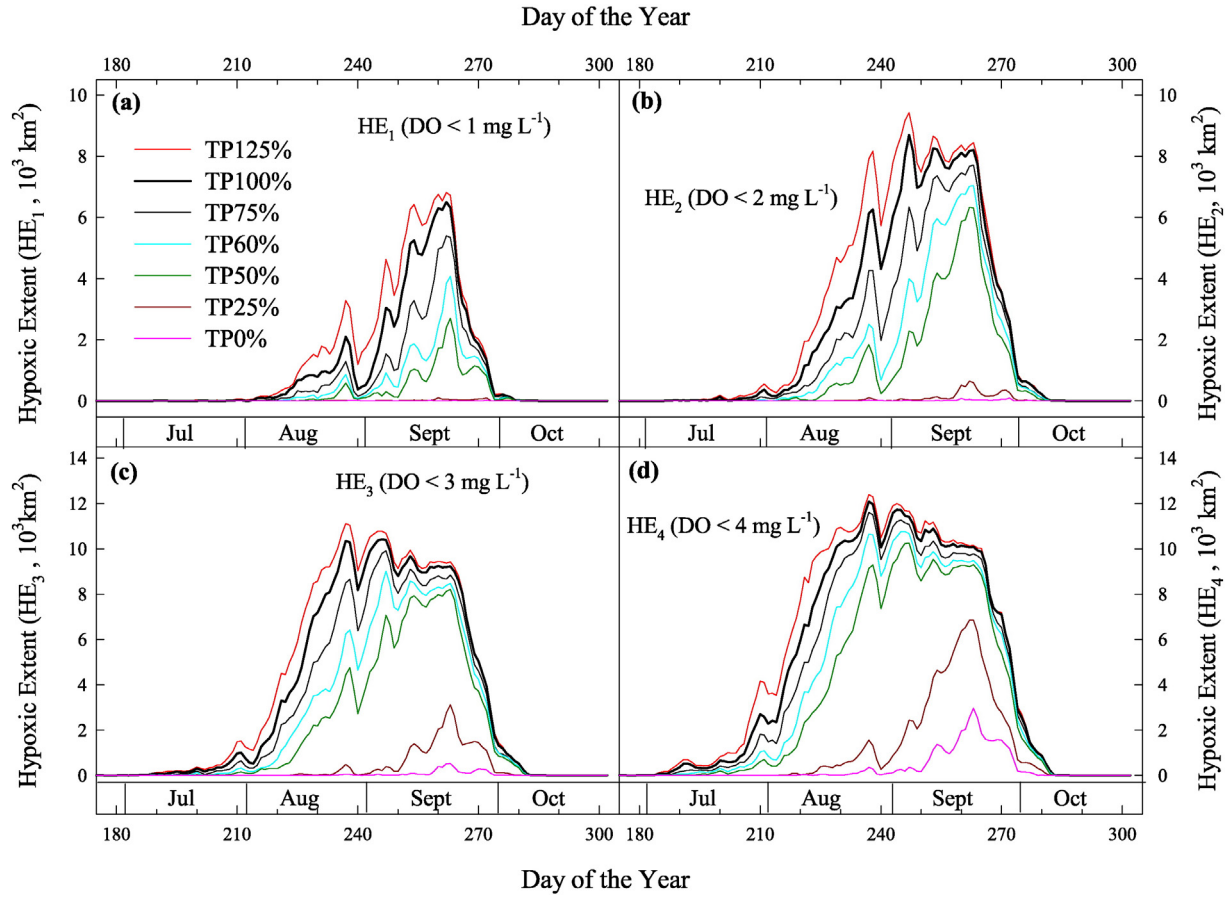

Fig. 5. Seasonal dynamics of hypoxic extents of different DO thresholds (HE_1, HE_2, HE_3, and HE_4) for different TP load scenarios relative to the 2008 load in (125%, $TP_{125\%}$; 100%, $TP_{100\%}$; 75%, $TP_{75\%}$; 50%, $TP_{50\%}$; 25%, $TP_{25\%}$; and, 0%, $TP_{0\%}$).

hypoxic extent, the effects of the load reduction on mean summer hypoxia are even larger. A 40% load reduction results in mean hypoxia extents reduced by 74.3% (1600 km^2), 42.6% (2000 km^2), 28.4% (2000 km^2) and 17.4% (1600 km^2) for HE_1, HE_2, HE_3 and HE_4, respectively (Fig. 8b). To reduce the mean area of HE_2 by half of the 2008 value the 44% reduction in nutrient load will be needed. Hypoxic

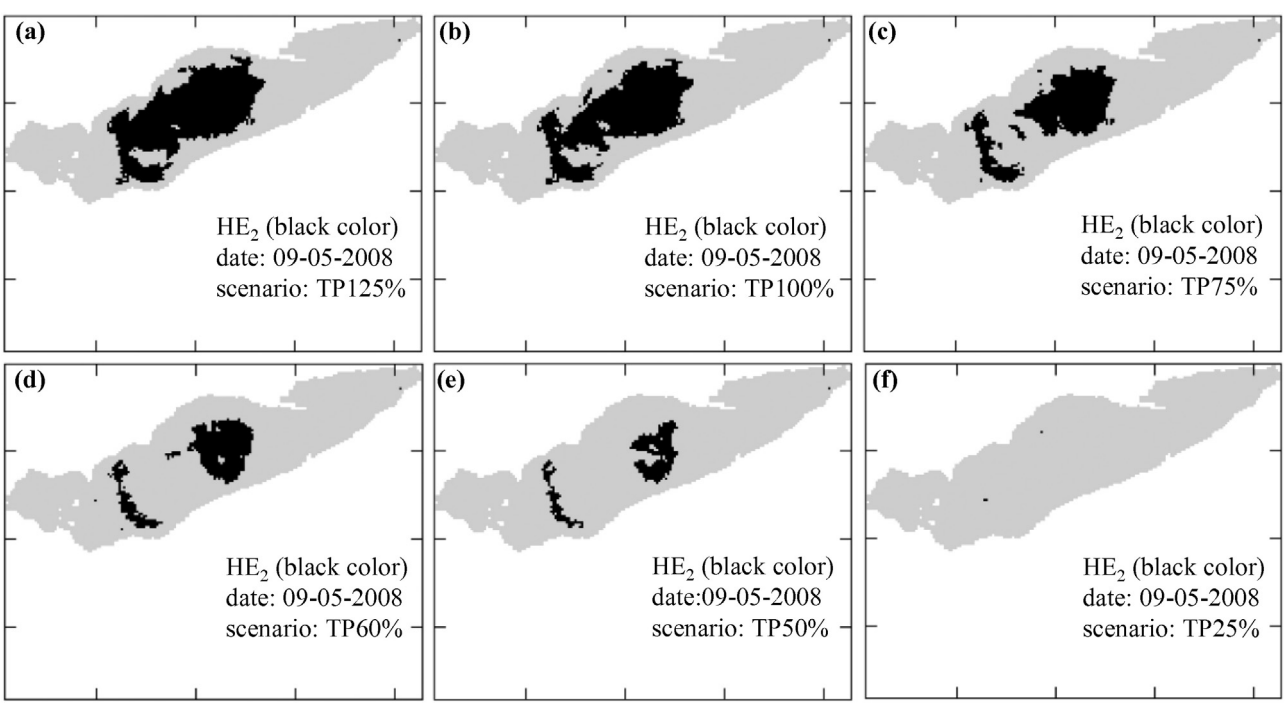

Fig. 6. Spatial extent of HE_2 (DO < 2 mg L^{-1}) on September 5 (DOY 249) for various nutrient loading scenarios: (a) $TP_{125\%}$, (b) $TP_{100\%}$, (c) $TP_{75\%}$, (d) $TP_{60\%}$, (e) $TP_{50\%}$, and (f) $TP_{25\%}$.

Please cite this article as: Bocaniov, S.A., et al., Simulating the effect of nutrient reduction on hypoxia in a large lake (Lake Erie, USA-Canada) with a three-dimensional lake model, J. Great Lakes Res. (2016), http://dx.doi.org/10.1016/j.jglr.2016.06.001

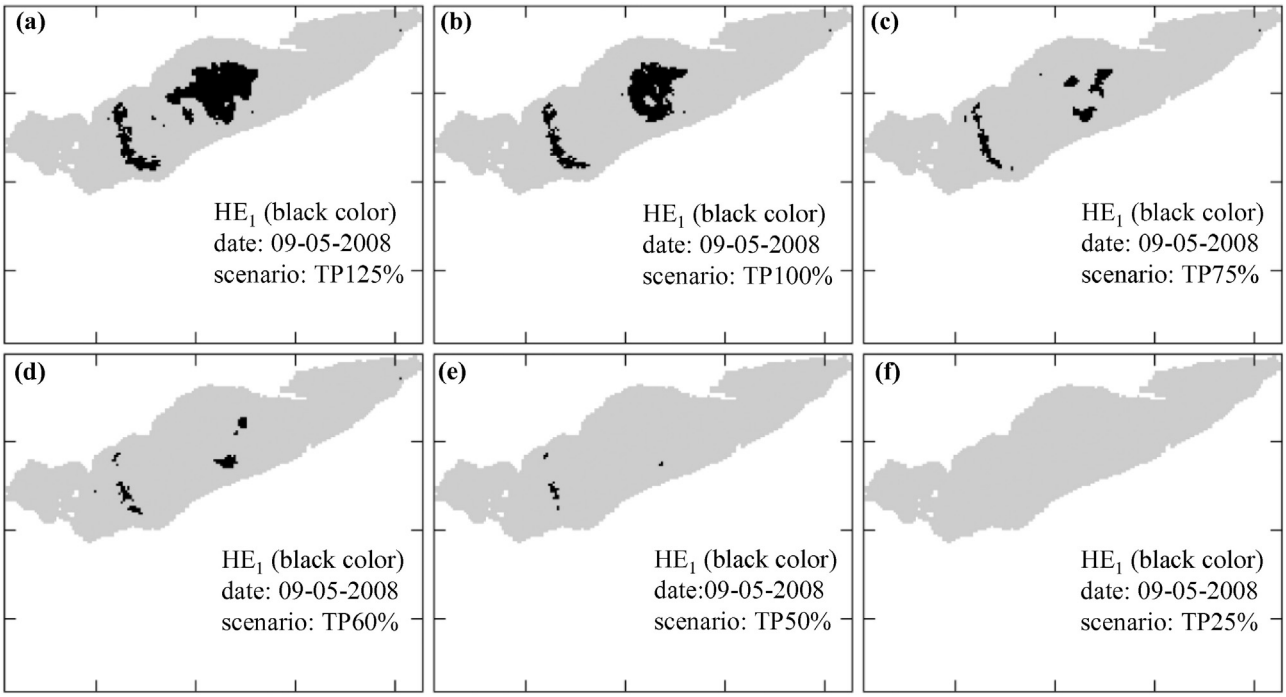

Fig. 7. Spatial extent of HE_1 (DO < 1 mg L^{-1}) on September 5 (DOY 249) for various nutrient loading scenarios: (a) $TP_{125\%}$, (b) $TP_{100\%}$, (c) $TP_{75\%}$, (d) $TP_{60\%}$, (e) $TP_{50\%}$, and (f) $TP_{25\%}$.

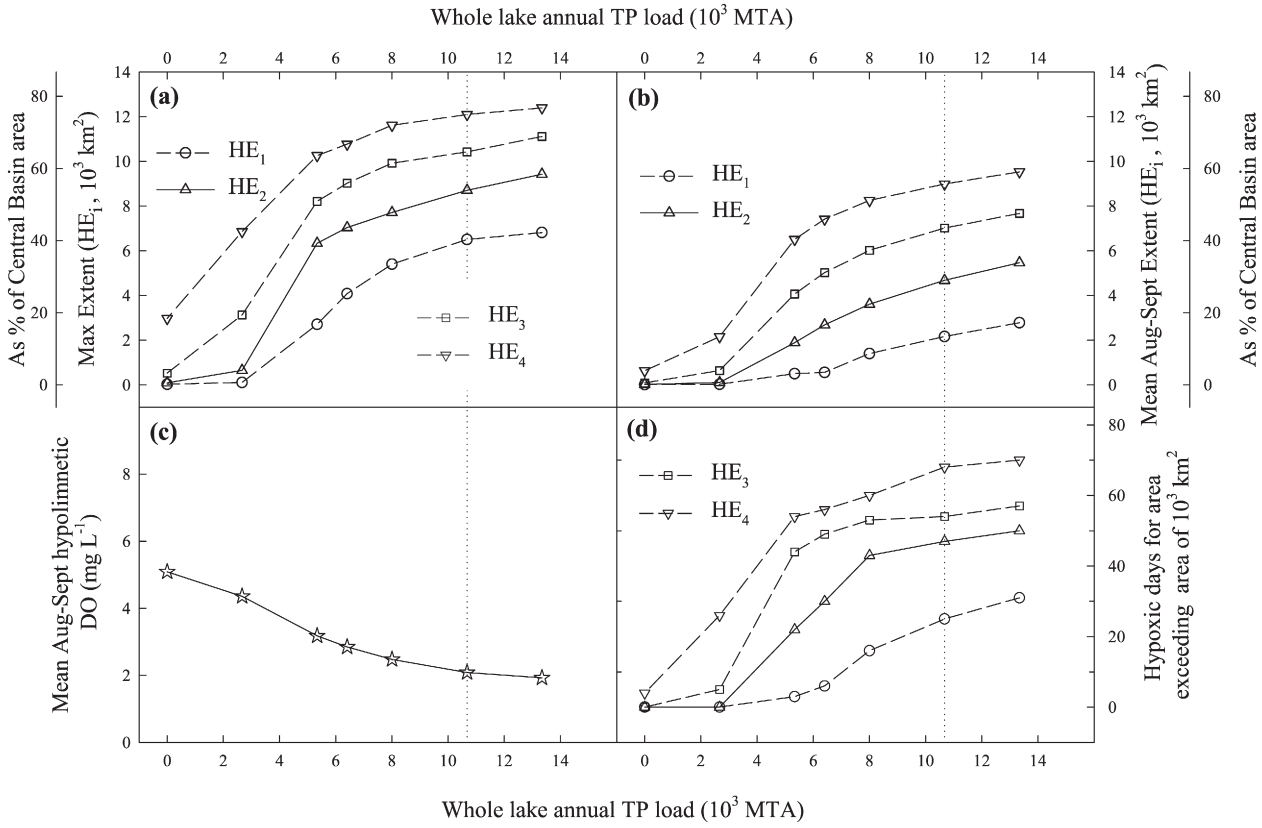

Fig. 8. Load response curves for different DO thresholds (HE_1, DO < 1 mg L^{-1}; HE_2, DO < 2 mg L^{-1}; HE_3, DO < 3 mg L^{-1}; HE_4, DO < 4 mg L^{-1}); maximum and mean (August–September) hypoxic extents (a, b); mean (August–September) hypolimnetic DO (c); and, duration of the hypoxia for an area that exceeds 10^3 km^2. The baseline scenario (2008 load) is indicated by vertical dotted line. MTA means metric tons per annum.

duration is also very sensitive to the chosen DO threshold. For a load reduction of 40%, the duration of hypoxic areas exceeding 2000 km^2 are reduced by 76% (25 vs 6 days), 36% (47 vs 30 days), 10% (54 vs 49 days) and 18% (68 vs 56 days), respectively (Figs. 5, 9 & 10; ESM Table S5). To reduce the duration of hypoxia exceeding the area of 2000 km^2 by half of its 2008 value the 48% reduction in nutrient load

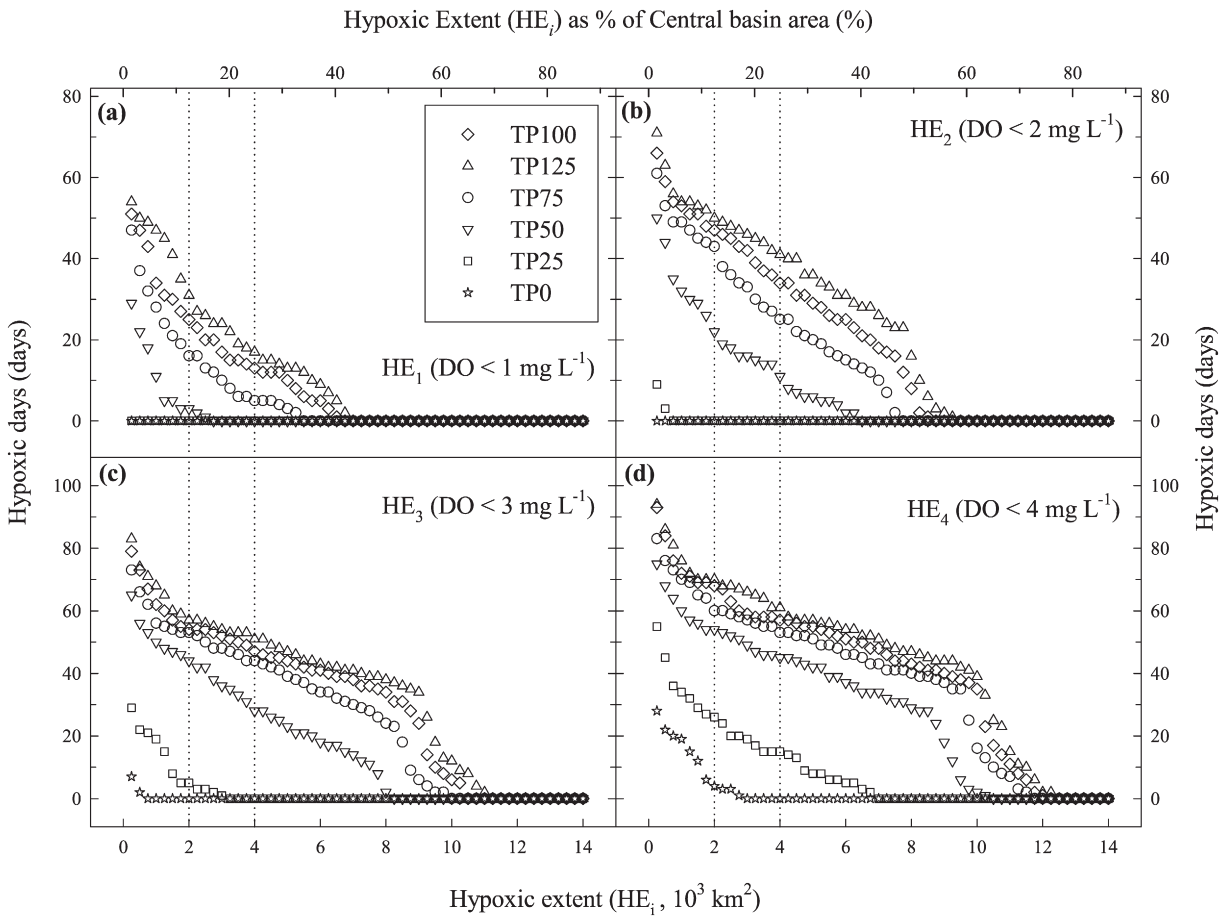

Fig. 9. Duration of hypoxia of different DO thresholds (HE_1: a; HE_2: b, HE_3: c; and, HE_4: d) when hypoxic zone exceeds any given specified area for various TP load scenarios. Vertical dotted lines indicate hypoxic extents of 2×10^3 and 4×10^3 km^2.

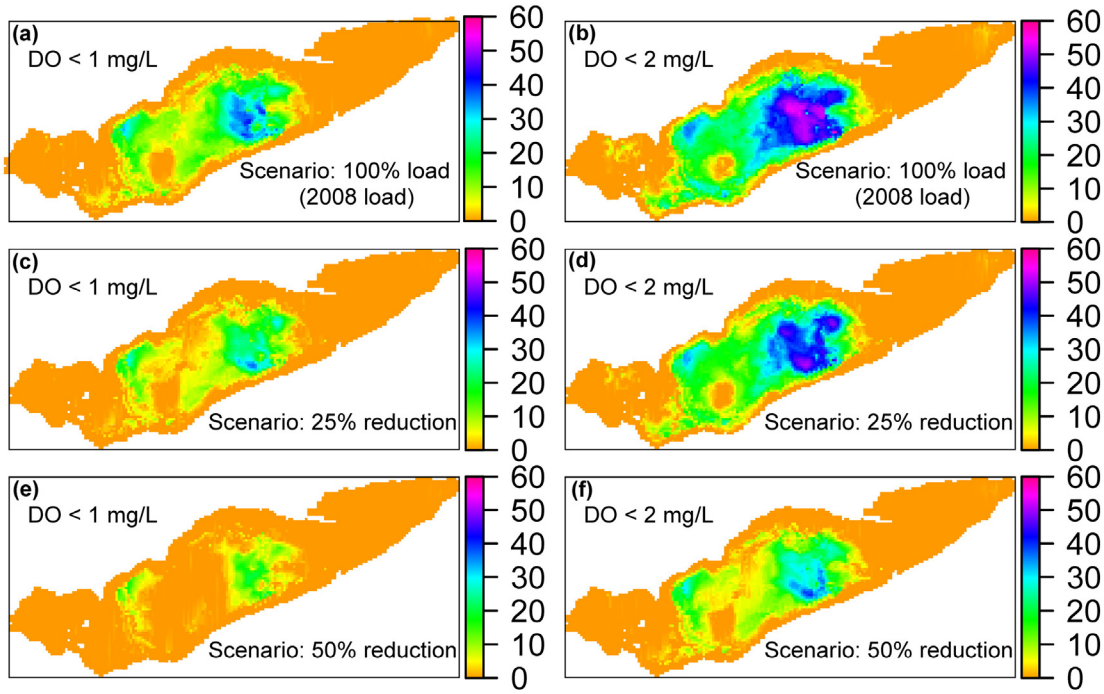

Fig. 10. Spatial plots of seasonally integrated hypoxia duration for two DO thresholds, 1 mg L^{-1} (a, c, e) and 2 mg L^{-1} (b, d, f), and for three selected load scenarios: $TP_{100\%}$ (a, b), $TP_{75\%}$ (c, d), and $TP_{50\%}$ (e, f).

Please cite this article as: Bocaniov, S.A., et al., Simulating the effect of nutrient reduction on hypoxia in a large lake (Lake Erie, USA-Canada) with a three-dimensional lake model, J. Great Lakes Res. (2016), http://dx.doi.org/10.1016/j.jglr.2016.06.001

must be achieved from the base case scenario (2008 levels). The reduction in external nutrient loads will not only reduce the extent and duration of hypoxic area but also help to reduce the occurrence and severity of harmful algal blooms in Lake Erie (e.g. Bertani et al., in this issue).

Acknowledgements

This work was funded in part by the University of Michigan Graham Sustainability Institute and the USEPA under contract EP-R5-11-07, Task Order 21.

Appendix A. Electronic Supplementary Material (ESM)

Supplementary data to this article can be found online at http://dx.doi.org/10.1016/j.jglr.2016.06.001.

References

Arend, K.K., Beletsky, D., DePinto, J.V., Ludsin, S.A., Roberts, J.J., Rucinski, D.K., ... Höök, T.O., 2011. Seasonal and interannual effects of hypoxia on fish habitat quality in Central Lake Erie. Freshw. Biol. 56 (2), 366–383.

Bastviken, D., Cole, J., Pace, M., Tranvik, L., 2004. Methane emissions from lakes: dependence of lake characteristics, two regional assessments, and a global estimate. Global Biogeochem. Cy. 18 (4), GB4009.

Beletsky, D., Hawley, N., Rao, Y.R., Vanderploeg, H.A., Beletsky, R., Schwab, D.J., Ruberg, S.A., 2012. Summer thermal structure and anticyclonic circulation of Lake Erie. Geophys. Res. Lett. 39, L06605.

Beletsky, D., Hawley, N., Rao, Y.R., 2013. Modeling summer circulation and thermal structure of Lake Erie. J. Geophys. Res. Oceans 118, 6238–6252.

Bertani, I., Obenour, D.R., Steger, C.E., Stow, C.A., Gronewold, A.D., Scavia, D., 2016. Probabilistically assessing the role of nutrient loading in harmful algal bloom formation in western Lake Erie. J. Great Lakes Res. (in this issue).

Bocaniov, S.A., Scavia, D., 2016. Temporal and spatial dynamics of large lake hypoxia: integrating statistical and three-dimensional dynamic models to enhance lake management criteria. Water Resour. Res. 52 (6), 4247–4263.

Bocaniov, S.A., Smith, R.E.H., Spillman, C.M., Hipsey, M.R., Leon, L.F., 2014a. The nearshore shunt and the decline of the phytoplankton spring bloom in the Laurentian Great Lakes: insights from a three-dimensional lake model. Hydrobiologia 731, 151–172.

Bocaniov, S.A., Ullmann, C., Rinke, K., Lamb, K.G., Boehrer, B., 2014b. Internal waves and mixing in a stratified reservoir: insights from three-dimensional modeling. Limnologica 49, 52–67.

Boegman, L., 2006. A model of the stratification and hypoxia in Central Lake Erie, p. 608–613. In: Ivey, G.N. (Ed.), Proc. 6th International Symposium on Stratified Flows, 11–14 Dec. IAHR, University of Western Australia.

Bolsenga, S., Herdendorf, C. (Eds.), 1993. Lake Erie and Lake St. Clair Handbook. Wayne State University Press.

Bouffard, D., Boegman, L., Rao, Y.R., 2012. Poincare wave-induced mixing in a large lake. Limnol. Oceanogr. 57 (4), 1201–1216.

Bouffard, D., Ackerman, J.D., Boegman, L., 2013. Factors affecting the development and dynamics of hypoxia in a large shallow stratified lake: hourly to seasonal patterns. Water Resour. Res. 49, 2380–2394.

Carlson, A.R., Blocher, J., Herman, L.J., 1980. Growth and survival of channel catfish and yellow perch exposed to lowered constant and diurnally fluctuating dissolved oxygen concentrations. Prog. Fish Cult. 42, 73–78.

CBMS, 2015. Chesapeake Bay management strategy, 2015–2025. Fish habitat outcome. Available online http://www.chesapeakebay.net/documents/22036/1c_fish_habitat_ms_6-24-15_ff_formatted.pdf (Assessed 12–28-2015).

Di Toro, D.M., Connolly, J.P., 1980. Mathematical models of water quality in large lakes. Part 2: Lake Erie, EPA-600/3-80-065 Report, Duluth, MN.

Di Toro, D.M., Thomas, N.A., Herdendorf, C.E., Winfield, R.P., Connolly, J.P., 1987. A post audit of a Lake Erie eutrophication model. J. Great Lakes Res. 13 (4), 801–825.

Farrell, A.P., Richards, J.G., 2009. Defining hypoxia: an integrative synthesis of the responses of fish to hypoxia. In: Richards, J.G., Farrell, A.P., Brauner, C.J. (Eds.), Hypoxia. Academic Press, London, pp. 487–503.

Gray, J.S., Wu, R.S.S., Or, Y.Y., 2002. Effects of hypoxia and organic enrichment on the coastal marine environment. Mar. Ecol. Prog. Ser. 238 (1), 249–279.

Guntenspergen, G.R. (Ed.), 2014. Application of Threshold Concepts in Natural Resource Decision Making. Springer (324 pp.).

Hawley, N., Johengen, T.H., Rao, Y.R., Ruberg, S.A., Beletsky, D., Ludsin, S.A., Eadie, B.J., Schwab, D.J., Croley, T.E., Brandt, S.B., 2006. Lake Erie hypoxia prompts Canada-U.S. study. Eos. Trans. AGU 87 (32), 313–319.

Hipsey, M.R., 2008. The CWR Computational Aquatic Ecosystem Dynamics Model CAEDYM. User Manual. Centre for Water Research (CWR), University of Western Australia.

Hodges, B., Dallimore, C., 2006. Estuary, Lake and Coastal Ocean Model: ELCOM. Science Manual. Centre of Water Research. University of Western Australia.

Hodges, B., Imberger, J., Saggio, A., Winters, K., 2000. Modeling basin-scale internal waves in a stratified lake. Limnol. Oceanogr. 45, 1603–1620.

Idso, S.B., Jackson, R.D., 1969. Thermal radiation from the atmosphere. J. Geophys. Res. 74, 5397–5403.

IJC (International Joint Commission), 1978. Great Lakes Water Quality Agreement of 1978, with annexes and terms of reference, between the United States and Canada. IJC: Windsor, Ontario, Canada, November 22, 1978.

IJC (International Joint Commission), 2012. Great Lakes Water Quality Agreement 2012. Protocol amending the agreement between Canada and the United States of America on Great Lakes water quality. IJC: Windsor, Ontario, Canada, September 7, 2012.

Jeppesen, E., Søndergaard, M., Jensen, J.P., Havens, K.E., Anneville, O., Carvalho, L., Coveney, M.F., Deneke, R., Dokulil, M.T., Foy, B.O.B., Gerdeaux, D., 2005. Lake responses to reduced nutrient loading–an analysis of contemporary long-term data from 35 case studies. Freshw. Biol. 50 (10), 1747–1771.

Jeppesen, E., Meerhoff, M., Jacobsen, B.A., Hansen, R.S., Søndergaard, M., Jensen, J.P., Lauridsen, T.L., Mazzeo, N., Branco, C.W.C., 2007. Restoration of shallow lakes by nutrient control and biomanipulation—the successful strategy varies with lake size and climate. Hydrobiologia 581 (1), 269–285.

Kraus, R.T., Knight, C.T., Farmer, T.M., Gorman, A.M., Collingsworth, P.D., Warren, G.J., ... Conroy, J.D., 2015. Dynamic hypoxic zones in Lake Erie compress fish habitat, altering vulnerability to fishing gears. Can. J. Fish. Aquat. Sci. 72 (6), 797–806.

Lam, D.C.L., Schertzer, W.M., Fraser, A.S., 1987. A post-audit anaylsis of the NWRI nine-box water quality model for Lake Erie. J. Great Lakes Res. 13 (4), 782–800.

Lam, D.C.L., Schertzer, W.M., McCrimmon, Charlton, M., Millard, S., 2008. Modeling phosphorus and dissolved oxygen conditions pre- and post-Dreissena arrival in Lake Erie. Checking the Pulse of Lake Erie. Backhuys Publ., Leiden, The Netherlands, pp. 97–121.

Leon, L.F., Smith, R.E.H., Hipsey, M.R., Bocaniov, S.A., Higgins, S.N., Hecky, R.E., Antenucci, J.P., Imberger, J.A., Guildford, S.J., 2011. Application of a 3D hydrodynamic-biological model for seasonal and spatial dynamics of water quality and phytoplankton in Lake Erie. J. Great Lakes Res. 37, 41–53.

Liu, W., Bocaniov, S.A., Lamb, K.G., Smith, R.E.H., 2014. Three dimensional modeling of the effects of changes in meteorological forcing on the thermal structure of Lake Erie. J. Great Lakes Res. 40, 827–840.

Maccoux, M., Dove, A., 2016. An update of TP loads to Lake Erie through 2013. J. Great Lakes Res. (in this issue).

Marsden, M.W., 1989. Lake restoration by reducing external phosphorus loading: the influence of sediment phosphorus release. Freshw. Biol. 21 (2), 139–162.

Oveisy, A., Rao, Y.R., Leon, L.F., Bocaniov, S.A., 2014. Three-dimensional winter modeling and the effects of ice cover on hydrodynamics, thermal structure and water quality in Lake Erie. J. Great Lakes Res. 40, 19–28.

Parkinson, C.L., Washington, W.M., 1979. A large-scale numerical model of sea ice. J. Geophys. Res. 84 (C1), 311–337.

Pena, M.A., Katsev, S., Oguz, T., Gilbert, D., 2010. Modeling dissolved oxygen dynamics and hypoxia. Biogeosciences 7 (3), 933–957.

Rao, Y.R., Howell, T., Watson, S.B., Abernethy, S., 2014. On hypoxia and fish kills along the north shore of Lake Erie. J. Great Lakes Res. 40, 187–191.

Roberts, J.J., Höök, T.O., Ludsin, S.A., Pothoven, S.A., Vanderploeg, H.A., Brandt, S.B., 2009. Effects of hypolimnetic hypoxia on foraging and distributions of Lake Erie yellow perch. J. Exp. Mar. Biol. Ecol. 381, S132–S142.

Roberts, J.J., Brandt, S.B., Fanslow, D., Ludsin, S.A., Pothoven, S.A., Scavia, D., et al., 2011. Effects of hypoxia on consumption, growth, and RNA:DNA ratios of young yellow perch. Trans. Am. Fish. Soc. 140, 1574–1586.

Rodgers, G.K., Anderson, D.V., 1961. A preliminary study of the energy budget of Lake Ontario. J. Fish. Res. Board Can. 18 (4), 617–636.

Rucinski, D.K., DePinto, J.V., Scavia, D., Beletsky, D., 2014. Modeling Lake Erie's hypoxia response to nutrient loads and physical variability. J. Great Lakes Res. 40, 151–161.

Rucinski, D.K., DePinto, J.V., Beletsky, D., Scavia, D., 2016. Modeling Lake Erie's hypoxia response to phosphorus load reduction scenarios. J. Great Lakes Res. (in this issue).

Sambridge, M., Braun, J., McQueen, H., 1995. Geophysical parametrization and interpolation of irregular data using natural neighbours. Geophys. J. Int. 122, 837–857.

Saylor, J.H., Miller, G.S., 1987. Studies of large-scale currents in Lake Erie, 1979–80. J. Great Lakes Res. 13 (4), 487–514.

Scavia, D., Allan, J.D., Arend, K.K., Bartell, S., Beletsky, D., Bosch, N.S., ... Zhou, Y., 2014. Assessing and addressing the re-eutrophication of Lake Erie: central basin hypoxia. J. Great Lakes Res. 40 (2), 226–246.

Scavia, D., DePinto, J., Bertani, I., 2016. A multi-model approach to evaluating target phosphorus loads for Lake Erie. J. Great Lakes Res. (in this issue).

Schertzer, W.M., Saylor, J.H., Boyce, F.M., Robertson, D.G., Rosa, F., 1987. Seasonal thermal cycle of Lake Erie. J. Great Lakes Res. 13 (4), 468–486.

Schwab, D.J., Morton, J.A., 1984. Estimation of overlake wind speed from overland wind speed: a comparison of three methods. J. Great Lakes Res. 10 (1), 68–72.

Sly, L.I., Hodgkinson, M.C., Arunpairojana, V., 1990. Deposition of manganese in a drinking water distribution system. Appl. Environ. Microbiol. 56 (3), 628–639.

Søndergaard, M., Jensen, P.J., Jeppesen, E., 2001. Retention and internal loading of phosphorus in shallow, eutrophic lakes. TheScientificWorldJOURNAL 1, 427–442.

Søndergaard, M., Jensen, J.P., Jeppesen, E., 2003. Role of sediment and internal loading of phosphorus in shallow lakes. Hydrobiologia 506 (1–3), 135–145.

State of Connecticut, 2015. Department of Energy and Environmental Protection Long Island Sound Water Quality Monitoring Program. http://tinyurl.com/paesg9v (Accessed 12-24-15).

Steckbauer, A., Duarte, C.M., Carstensen, J., Vaquer-Sunyer, R., Conley, D.J., 2011. Ecosystem impacts of hypoxia: thresholds of hypoxia and pathways to recovery. Environ. Res. Lett. 6 (2), 025003.

USEPA (United States Environmental Protection Agency), 1986. Quality criteria for water -1986. (EPA 440/5-86-001). USEPA, Washington, DC.

Vanderploeg, H.A., Ludsin, S.A., Ruberg, S.A., Höök, T.O., Pothoven, S.A., Brandt, S.B., Lang, G.A., Liebig, J.R., Cavaletto, J.F., 2009. Hypoxia affects spatial distributions and overlap

of pelagic fish, zooplankton, and phytoplankton in Lake Erie. J. Exp. Mar. Biol. Ecol. 381, S92–S107.
Vaquer-Sunyer, R., Duarte, C.M., 2008. Thresholds of hypoxia for marine biodiversity. Proc. Natl. Acad. Sci. 105 (40), 15452–15457.
Zhang, H., Boegman, L., Xu, X., Briland, R., Culver, D., 2016. Spatiotemporal distributions of phosphorus loads and their impacts on Lake Erie's water quality. J. Great Lakes Res. (in this issue).
Zhou, Y., Obenour, D.R., Scavia, D., Johengen, T.H., Michalak, A.M., 2013. Spatial and temporal trends in Lake Erie hypoxia, 1987–2007. Environ. Sci. Technol. 47, 899–905.
Zhou, Y., Michalak, A.M., Beletsky, D., Rao, Y.R., Richards, R.P., 2015. Record-breaking Lake Erie hypoxia during 2012 drought. Environ. Sci. Technol. 49 (2), 800–807.

Please cite this article as: Bocaniov, S.A., et al., Simulating the effect of nutrient reduction on hypoxia in a large lake (Lake Erie, USA-Canada) with a three-dimensional lake model, J. Great Lakes Res. (2016), http://dx.doi.org/10.1016/j.jglr.2016.06.001